FULL PAPER

Role of fluid on seismicity of an intra-plate earthquake zone in Western India: an electrical fingerprint from magnetotelluric study

Ujjal K. Borah[1,2], Prasanta K. Patro[2*], Khasi Raju[2,4], K. Chinna Reddy[2], Narendra Babu[2], P. Rama Rao[3] and N. Purnachandra Rao[2]

Abstract

The magnetotelluric (MT) investigation carried out in Koyna Seismogenic Zone (KSZ), an intra-plate earthquake region in Western India, along an E–W profile brings out moderately conductive (~ 700–1000 Ωm) near vertical features within the very high resistive (> 20,000 Ωm) granite/granite-gneiss basement. Occurrences of these anomalous moderate conductors are corroborated with sensitivity analysis. The alignment of earthquake hypocenters along the resistive–conductive boundary signifies the moderate conductor as basement fault. The conversion of resistivity values to the ratio of seismic P- to S-wave velocity (v_p/v_s) suggests that the moderate conductivity of the fault zone (as compared to the surrounding basement) appears due to the presence of fluid in the fault zone. Geophysical evidences reveal ~ 2.5–3.6 vol% fluid in the fault zone with ~ 1.8–2.6% interconnected porosity, which migrates along the structural boundary and invades the mechanically strong basement to nucleate the brittle failure within it. The present study proposes two mechanisms for the seismicity in the Koyna region. First: the meteoric water circulation due to the loading–unloading of nearby Koyna reservoir acts as potential fluid source for this triggered seismicity, which has also been suggested by previous studies. Second: the fluid circulation due to a deep-seated source. The present MT study brings out a conductive feature below 20 km depth which is thought to be emerged due to the dehydration of amphibole bearing rocks. The fluid generated from dehydration might act as a probable source to the triggered seismicity; since the conductive feature has a linkage to the upper crust.
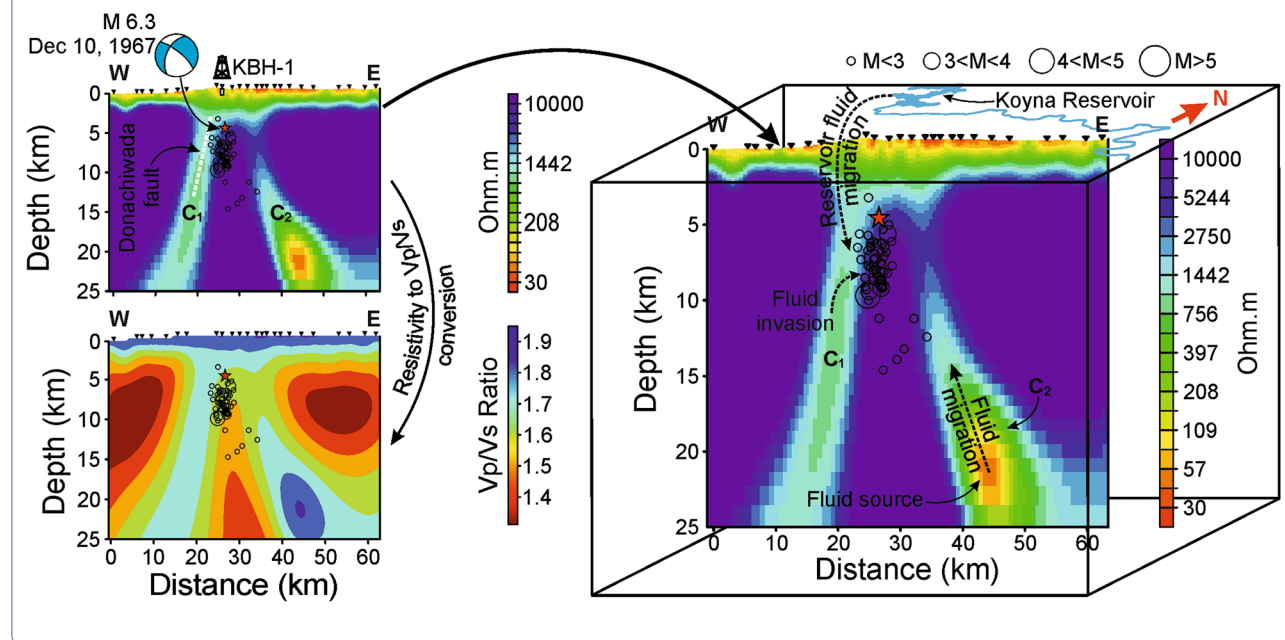
Keywords Koyna Seismogenic Zone, Magnetotellurics, Resistivity, Fluid, Triggered seismicity, Seismotectonic

*Correspondence:
Prasanta K. Patro
patrobpk@ngri.res.in
Full list of author information is available at the end of the article

Graphical Abstract

Introduction

Potential role of fluid, originated from mantle dehydration reaction (Fulton and Saffer 2009) or partial melt associated with aqueous fluid (Schilling and Partzsch 2001), is observed in earthquake processes (Miller 2013) along plate boundaries and volcanic arcs (Irwin and Barnes 1980) at lower crustal to upper mantle depth. However, in the upper crustal level, fluid associated with artificial reservoir impoundment (Gupta 2002, 2011; Gupta et al. 2017), fluid injection (Chen et al. 2017) are primary causes for triggering earthquakes in an intraplate region. Koyna Seismogenic Zone (KSZ) in Western India is such an intra-plate earthquake zone (Fig. 1). Micro-earthquakes were observed in KSZ in conjunction with the dam construction on Shivajinagar Lake (Koyna reservoir in Fig. 1) in the early 1960s (Pandey and Chadha 2003). However, the impoundment of Koyna reservoir (Fig. 1) in 1962 boosted up the micro-seismicities and KSZ started to experience earthquakes of $M \geq 3$, after the water column attained the average height in 1963 (Guha et al. 1968; Pandey and Chadha 2003), and leads to the occurrence of a $M \sim 6.3$ earthquake (Gupta et al. 1969) in Koyna (Fig. 1). These seismic activities have been continuing for the last five decades.

The occurrence of the devastating December 10, 1967 Koyna earthquake (M 6.3) became special interest for the scientific community as it occurred in a nearly non-seismic (Gupta et al. 1969) intra-plate zone. Therefore, a set

of possible concepts for the earthquake genesis came forward, e.g. reservoir triggered seismicity (RTS) by Narain and Gupta (1968a, b), Gupta et al. (1969) and Gupta (1983); rift valley structure by Krishna Brahmam and Negi (1973); strain released from a probable fault along west coast of India by Athavale and Mohan (1976); vertical movement of crustal block by Kailasam et al. (1976) etc. However, based on the correlation between earthquake occurrence frequency and RTS characteristics (such as increment rate of reservoir water level, highest point that the reservoir water level achieves, duration of retention of high water level), Gupta et al. (1969, 1972a, b, 2002); Gupta and Rostogi (1974, 1976); Gupta (1983) suggested that the continuous seismic activities in Koyna region are related to RTS. Though these studies have suggested the continuous earthquakes as RTS events, the triggering mechanism is still little understood (Gupta et al. 2015).

Electrical resistivity, a physical parameter, has a vital role in studying such fluid-triggered earthquakes. Fluids (aqueous fluids/partial melts) are associated with very low electrical resistivity and a small amount of fluid within a rock matrix considerably reduces its bulk resistivity. In addition, fluids strongly affect the deformation mechanisms and rheology of the rocks (Burgmann and Dresen 2008). Therefore, estimation of subsurface electrical resistivity will help to determine the zone of saturation and its interconnectivity; constrain the subsurface fluid
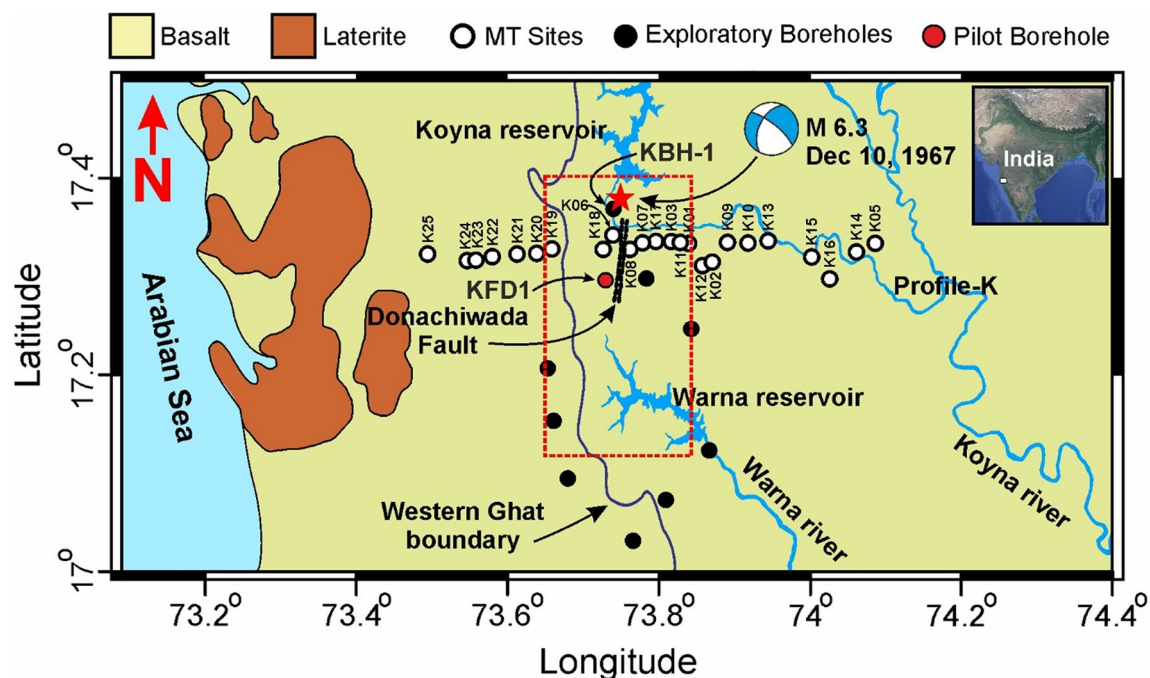
Fig. 1 Location map showing the geology (input taken from Geological Survey of India) of KSZ. The seismic activity of KSZ is restricted to ~ 30 km × 20 km area (Gupta et al. 2015) which approximately covers the region between the Koyna reservoir in the north and the Warna reservoir in the south (red coloured dashed blok). The white circles represent the MT stations (profile-K, near M 6.3 December 10, 1967 earthquake). The black circles represent the positions of exploratory boreholes drilled to instal borehole seismometer (Gupta et al. 2017). The red circle represents the position of the 3-km-deep pilot borehole (Goswami et al. 2020)

volume and the rheology (Becken et al. 2011). Therefore, the electrical investigation in KSZ is crucial. However, a very few electrical and electromagnetic (EM) investigations (Kailasam et al. 1976; Patro and Sarma 2009; Sarma et al. 2004) are carried out till date to get electrical signature of the subsurface of KSZ. These limited studies were carried out in large scale, which just touched the Koyna region with few stations and therefore, provide very little electrical information of KSZ. As magnetotelluric (MT), a passive EM geophysical technique, can give electrical image with a wide depth range and proves to be effective in basalt covered areas, we, therefore, have chosen MT method to delineate KSZ in detail. A broad band MT survey is carried out along an E–W profile across the KSZ (profile-K, Fig. 1). The acquired data are inverted two dimensionally (2D) to evaluate the detailed sub-basalt upper crustal geoelectrical structures along the E–W profile. The derived electrical signatures are then analysed for the geophysical evidences of fluid role on triggering earthquakes/brittle failure and related seismicity.

Geologic and tectonic setting

The study area, KSZ is situated on an N–S elevated escarpment called Western Ghats that runs parallel to the west coast of India (Fig. 1). Almost all the area is covered by ~ 67.4 Ma old Deccan basalt (Duncan and Pyle 1988), which comprised of sequential lava flows. Each basaltic lava flow comprises brecciated layer followed by a vesicular and/or amygdaloidal layer and then a fine-grained massive basalt layer (Roy et al. 2013). The Deccan basalts are underlain by Archean crystalline granite/granite-gneiss basement (Sarma et al. 2004). The Donachiwada fault (Gupta et al. 1999), associated with the December 10, 1967 Koyna earthquake (M 6.3), is striking approximately in an NNE–SSW direction (black dashed lines, Fig. 1). From the fault plane solution study (Langston and Franco-Spera 1985) Donachiwada fault is found as strike slip in nature and surficial evidences indicated towards a left-lateral movement (Talwani 1997). Drilling in this NNE–SSW trending Donachiwada fault suggested a dip amount of 60° WNW (Gupta et al. 1999). The wellbore breakouts and drilling-induced tensile fractures (DITFs) observed in a 3 km deep borehole (KFD1, Goswami et al. 2020) in KSZ (Fig. 1) constrain N9°W ± 17° mean orientation for the maximum horizontal principal stress, S_{Hmax} (Goswami et al. 2020) which is subparallel/oblique to

Borah *et al. Earth, Planets and Space*   (2023) 75:149

Page 4 of 14

the strike of Donachiwada fault. The direction of S_{Hmax} is consistent with the NW oriented crustal stress field in the Southern India as determined from rock mechanics studies (Gowd et al. 1992).

Magnetotelluric data and analysis

MT data are acquired in a rolling array pattern with constantly maintained remote site for most of the survey duration. ADU07e instrument is deployed to acquire the orthogonal electric and magnetic field for the period range 0.001–100 s. The MT data at few locations were affected due to electrical noise as this region is traversed by many high-tension power lines and contaminated with other cultural noise. We, therefore, adopt the systematic processing work flow of Borah et al. (2015) to handle the noise and improve the S/N ratio of the datasets (see Fig. 2 for example of data quality). The consistency of the processed resistivity and the phase data is examined with D$^+$ approach of Beamish and Travassos (1992) assigning 10% and 5% error to apparent resistivity and phase data, respectively (Fig. 2).

Dimensionality and regional strike analysis

In MT method, the observed data are being checked for dimensionality before adopting a particular modelling approach to convert the observed MT impedances to a true resistivity subsurface section (Simpson and Bahr 2005). The rotationally invariant dimensionality parameter Swift Skew, κ (Swift 1967) is especially sensitive to the static shift effect (occur due to local, near surface inhomogeneities), hence, leads to the incorrect interpretation of one dimensional (1D) or 2D structure as three dimensional (3D) structure (Jones 2012). Therefore, we have tested the dimensionality of our data set with Bahr Phase Sensitive Skew, η (Bahr 1988); a dimensionality measurement based on the phases of the impedance tensor and thus, unaffected by static shift effect. According to Bahr (1988, 1991), $\eta > 0.3$ represents a 3D structure. Figure 3a describes dimensionality of the data in terms of η at each period of a station along the profile. It is observed that, for most of the sites, the values of η are within the threshold limit of 0.3 up to 10 s, suggesting 1D/2D nature of the subsurface beneath the profile. The scattered high (> 0.3) η values observed in the short period (0.001–0.01 s) are the indication of noise contamination in the impedance data. Further, we also estimate the phase tensors (PT) ellipses (Caldwell et al. 2004) filled with β-values (skew angle) for each period of all MT sites along the profile. It is observed that for most of the sites, the PT plots for period < 10 s are circular to elliptical in shape and associated with β-values that are close to zero, which indicates a 2D subsurface up to 10 s. PT ellipses plot at three periods for all the MT stations are presented in Fig. 3b. Both η and PT analysis mostly suggest that the subsurface along the profile is 2D up to 10 s.

Accumulation of electric charge at the interface of near surface inhomogeneities produces secondary electric field and that distorts the measured MT responses; therefore, such MT responses are unable to represent the regional conductivity structure precisely. This problem of distortion can be minimized by applying tensor decomposition technique (Becken and Burkhardt 2004; Groom and Bailey 1989; McNeice and Jones 2001; Smith 1995, 1997) which separates local scale galvanic effect from the MT responses and in the 2D situation, gives regional geoelectrical strike direction. Therefore, in our study, we have adopted the single-site multi-frequency approach (McNeice and Jones 2001) which is based on the decomposition method of Groom and Bailey (1989) for regional geoelectrical strike estimation. It may be seen that the difference (RMS error) between the 2D decomposed responses (McNeice and Jones 2001) and the observed
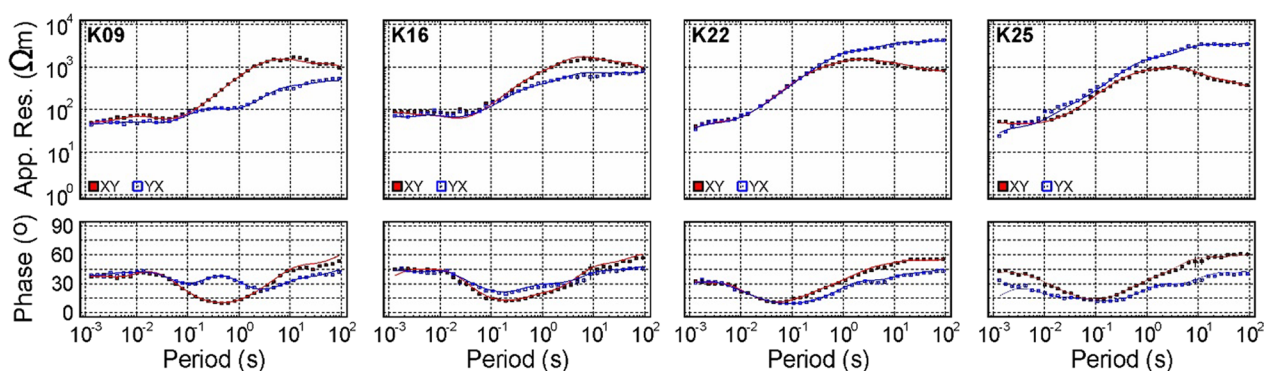

Fig. 2 Example of data in terms of apparent resistivity and phase with increased S/N ratio after systematic processing (Borah et al. 2015) show a good consistency through D$^+$ approach (solid blue and red lines) of Beamish and Travassos (1992). Remaining data of all the sites are given in Additional file 1: Fig. S1
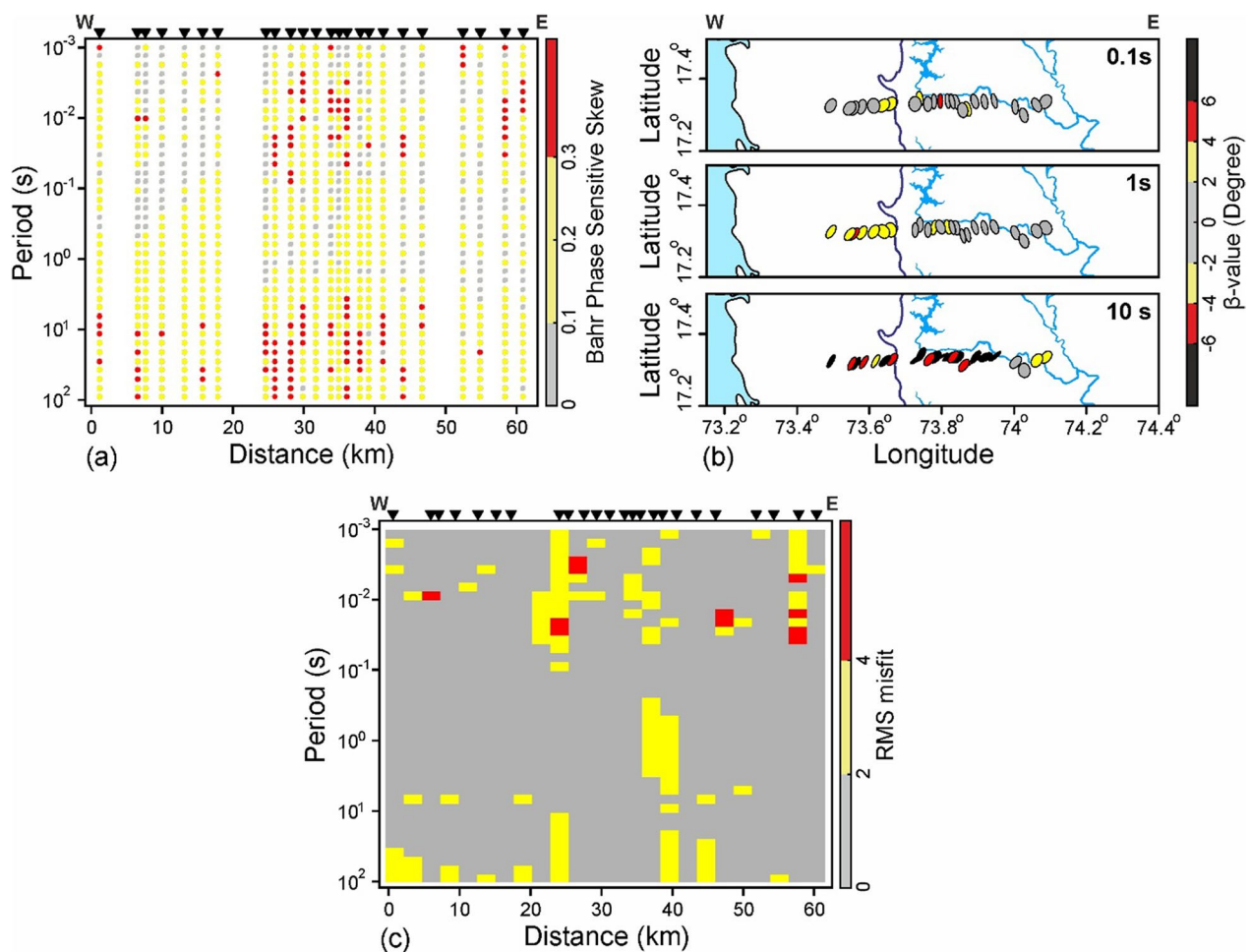
Fig. 3 Dimensionality analysis for the acquired data in KSZ. **a** Bahr Phase Sensitive Skew (Bahr 1988) plot at each period of each site along the profile. An overall low skew value (< 0.1) is observed at the shorter periods with few outliers. Bahr Skews have intermediate values (0.1–0.3) up to 10 s represent a 2D earth up to 10 s. **b** Phase tensor, PT (Caldwell et al. 2004) filled with β-value plots at three periods (0.1 s, 1 s and 10 s) for all the sites along the profile. Up to period 10 s PTs are circular to elliptical in shape with β-values close to zero which represents a 2D subsurface up to 10 s. **c** RMS misfit plot between 2D decomposed responses (McNeice and Jones 2001) and observed data. An overall low RMS value (≤ 2) is observed for period range 1–10 s of all the sites validating 2D subsurface for this period range
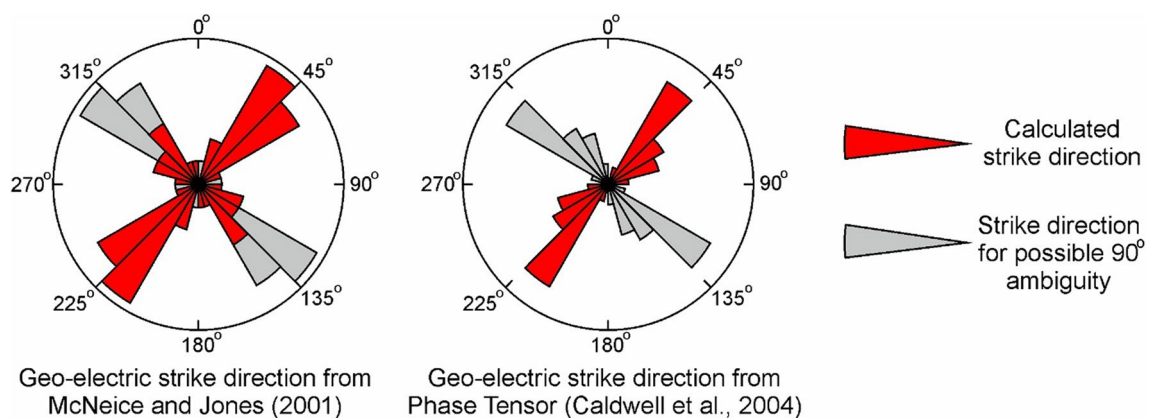

Fig. 4 Rose diagram showing the geoelectrical strike direction as estimated from tensor decomposition (McNeice and Jones 2001) and phase tensor (Caldwell et al. 2004), along with the inherent 90° ambiguity in strike estimation for the period band 1–10 s. The red and grey wedges of rose diagram represent the two possible mutually perpendicular geoelectrical strike direction
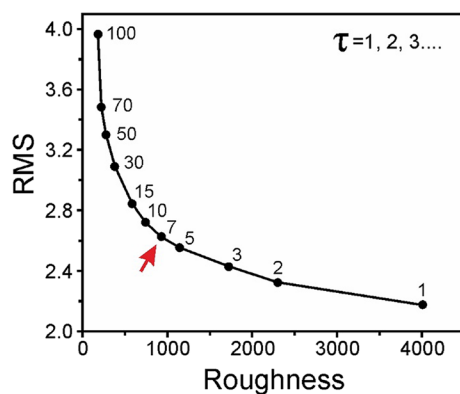
Borah *et al. Earth, Planets and Space* (2023) 75:149

Page 6 of 14

Fig. 5 L-curve obtained for profile-K with the systematic variation of regularization parameter (τ). Here $\tau = 7$ is fixed as reliable regularization parameter for the profile
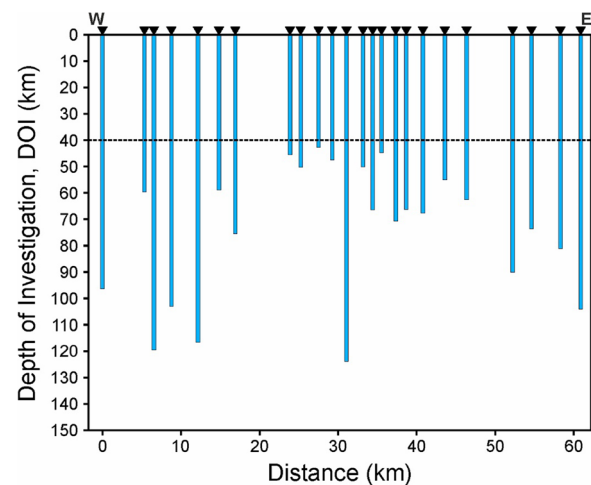

Fig. 6 DOI (Borah and Patro 2019) estimated from the average phase of TE and TM mode data of period 10 s for each station along the profile

data throughout the period ranging from 1 to 10 s for almost all the sites is low (≤ 2), which strongly validates the 2D assumption (Fig. 3c). Although galvanic distortion distorts the observed electric field amplitude, the phase between electric and magnetic (horizontal) field is virtually unaffected (Caldwell et al. 2004). We, therefore, also adopted the PT approach (Caldwell et al. 2004) to estimate the strike direction. The main advantage of PT analysis is that, it does not require the assumption about the dimensionalities of the subsurface conductivity structures like the other techniques (Caldwell et al. 2004).

Dimensionality analysis (both η and PT) of MT data and RMS misfit between decomposed responses and the observed data (Fig. 3) suggests a 2D subsurface up to period 10 s, therefore, to estimate the regional strike we consider the period range 1–10 s (mostly upper crustal depths). For our data set a predominant geoelectrical strike in NE–SW direction ($\sim$ N33°E) is obtained from both McNeice and Jones (2001) and PT analysis (Caldwell et al. 2004) for the period range 1–10 s (Fig. 4). The Donachiwada fault (Gupta et al. 1999; Shashidhar et al. 2013) follows the same trend as calculated strike (see Fig. 1) and hence we finalize the strike N33°E for the profile. After getting the proper strike direction, we rotate the measured impedance tensors of all MT sites to align the *XY* components of impedance tensor (Z_{XY}) along the strike. This aligned *XY*-component after rotation is assigned to *E* polarization (TE mode) and the rotated *YX* component is assigned to *B* polarization (TM mode).

Two-dimensional (2D) inversion

In the present study, we use the 2D inversion scheme Non-Linear Conjugate Gradient (NLCG) algorithm of Rodi and Mackie (2001) to bring out the 2D upper-crustal geoelectrical structures along profile-K. A homogeneous half space of 100 Ωm background resistivity having exact topography variation along the profile is taken as the initial model to start the iterative NLCG algorithm. Arabian Sea is situated 25–30 km away from the western most MT sites (Fig. 1). Hence, to tackle the effect of the highly conductive water mass (ocean) on the measured impedance tensor, we fix the ocean with its exact bathymetry and position in the initial 100 Ωm background grid and assigned a resistivity value of 0.33 Ωm to the fixed ocean.

The non-uniqueness of MT inversion (Constable et al. 1987; Jones and Hutton 1979; Oldenburg et al. 1984; Parker and Whaler 1981) can be constrained with regularization, which search for a model that has minimum misfit between the observed and predicted data and also tries to keep the model smooth as possible (Tikhonov and Arsenin 1977). In NLCG algorithm, the regularization parameter (τ) influences both the data fit and the model roughness. If τ is small, data fit will be good but the model will not be a smooth one and vice versa. Therefore, to get a reliable τ value which can take care of both the data fit and model roughness, we applied different τ values and carried out the inversion keeping the other parameters constant. The data fit (RMS error) is then plotted against the model roughness for each τ value (Fig. 5). According to Hansen (1998), this plotting will give an *L*-shaped trade-off curve and the reliable τ value which has a good agreement with data fit and model roughness will take its position at the knee of the curve. From the *L*-curves plotted for profile-K (Fig. 5), $\tau = 7$ is considered to be the reliable value.

Both TE and TM mode data for the period range 0.001–10 s are inverted jointly applying NLCG algorithm (Rodi and Mackie 2001), taking regularization parameter,
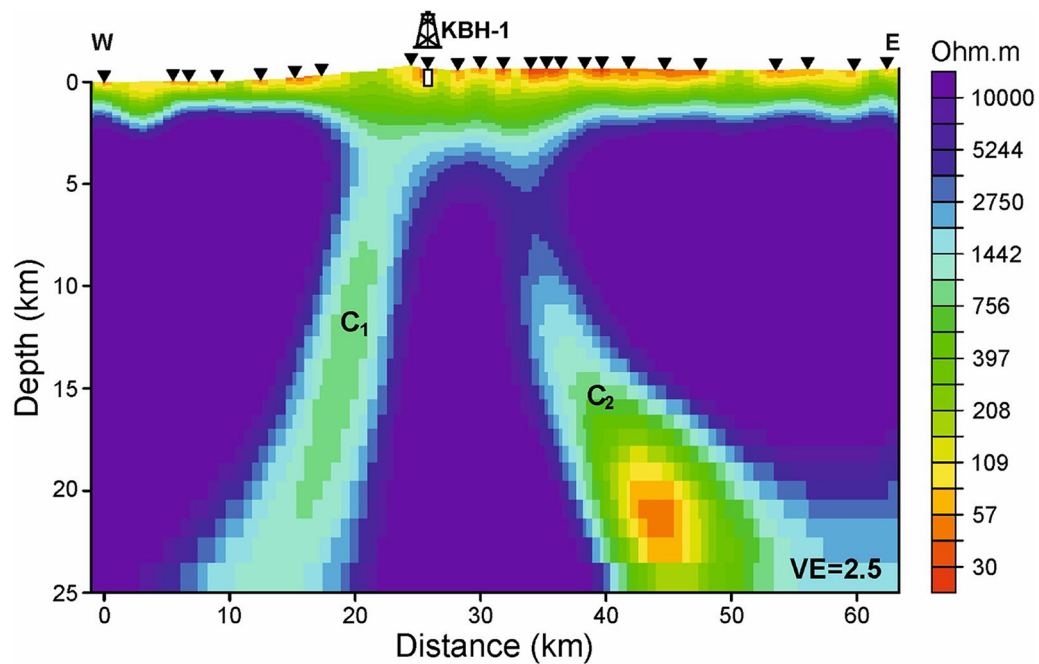
Fig. 7 2D inversion output from joint inversion of TE and TM data along profile-K using NLCG algorithm of Rodi and Mackie (2001) for period range 0.001–10 s up to 25 km (VE = 2.5) depth. The Deccan Trap thickness obtained from inversion is compared with the nearby borehole data (KBH-1, see Fig. 1) and found that it is well consistent with drilling result
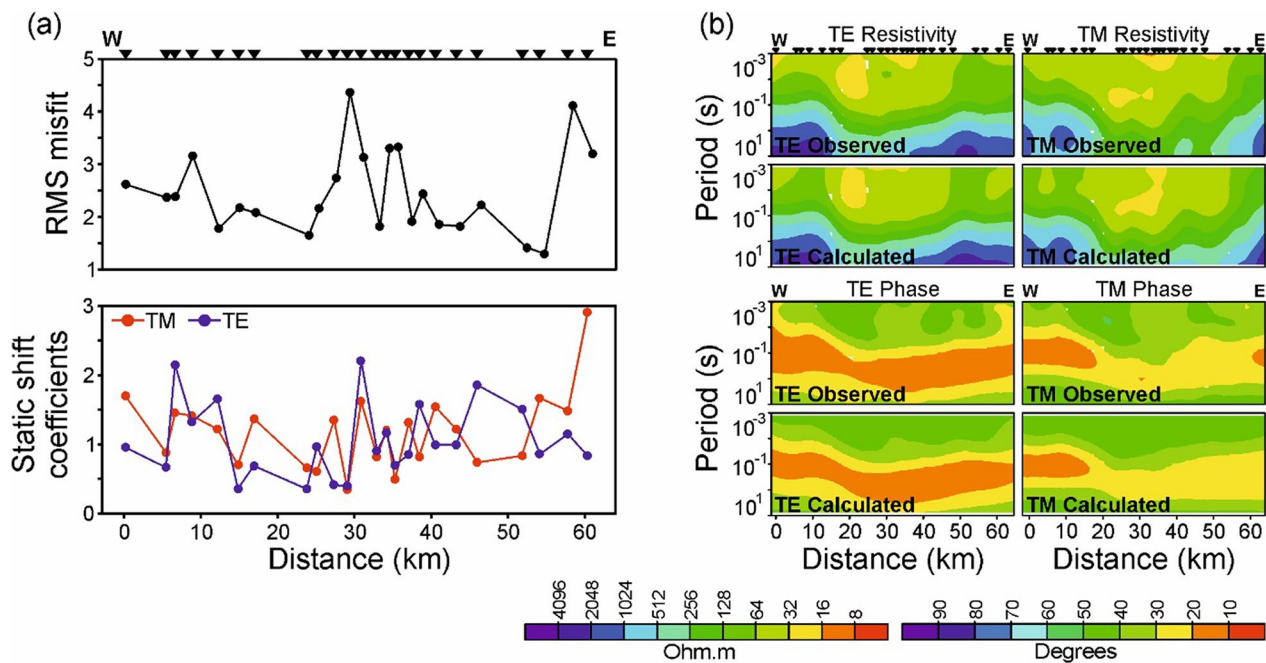

Fig. 8 a RMS misfit (top) and static shift coefficients (bottom) computed during inversion at each station along profile-K where 1 represents no static shift. **b** Pseudo-sections representing the comparison between observed and computed responses of TE and TM data along profile-K

$\tau = 7$ and assigning 20% error floor to apparent resistivity and 5% error floor to phase and get the smooth model after 100 iterations. The static shift coefficients (the real scaling factors by which the apparent resistivity curves are shifted relative to each other due to near surface inhomogeneities) at each station along the profile are computed during inversion and are corrected from the responses of this model by carrying out the inversion for further 30 more iterations. The final inverted 2D model obtained after 130 iterations yielded an RMS error of 2.53. Before evaluating this derived 2D model, we have computed the depth of investigation (DOI) of each station (Fig. 6) using the average phase of TE and TM mode data associated with 10 s period using the formula derived by Borah and Patro 2019. It is seen that all the stations have more than 40 km of DOI (Fig. 6) and therefore, we consider our final inverted 2D model along profile-K up to 25 km depth (Fig. 7; vertical exaggeration, VE = 2.5) for further analysis and interpretation.

The limit up to which the measured MT data are reconstructed by the model responses of the inversion output is expressed numerically in terms of RMS misfit. The overall RMS misfits at each station along the profile are presented in Fig. 8a (top) along with the static shift coefficients Fig. 8a (bottom). It may be seen that there is good agreement between static shift and RMS misfit; high RMS values coincide with high static shift values (Fig. 8a). To have a vivid view of the data misfit, we have plotted the measured data and computed responses at each station along the profile as pseudo-section (Fig. 8b). The observed and computed responses fit well for both TE and TM data (Fig. 8b).

Results

It is observed that the 2D inversion of MT data along profile-K (Fig. 7) brings out the relatively conductive ($\approx$ 30 Ωm) Deccan basalt cover on the top and very high resistive ($\geq 20{,}000$ Ωm) Archean granite/granite-gneiss basement (Sarma et al. 2004) beneath. The thickness of the Deccan basalt delineated from the 2D inversion is consistent with the scientific drilling result (Gupta et al. 2017) (Fig. 7). The very high resistive basement is cut by anomalous near vertical, moderately conductive ($\approx$ 700–1000 Ωm) features (C_1 and C_2 in Fig. 7) which separates the basement into different blocks.

In order to test the reliability of C_1, and C_2 (Fig. 7), we have carried out sensitivity analysis. First, the resistivity values of C_1, and C_2 obtained in the static shift corrected final inversion model (Fig. 7) are changed to the resistivity of the adjacent part. For this set up, the inversion is run for further 100 more iterations to examine whether the signatures of C_1, and C_2 are retrieved or not. After completion of 100 iterations, it is seen that the

expressions of C_1, and C_2 reappear (Fig. 9a). Secondly, forward responses are generated on the final static shift corrected inverted model with the resistivity of C_1 and C_2 changed to the resistivity of the adjacent part. These forward responses are then compared with the model responses of the inversion output along with the data. The comparison study of the responses at those sites (K18, K03) which fall near the moderately conductive zones shows that the data fit degrades if resistivities of C_1, and C_2 are changed to high resistivity of the adjacent part (Fig. 9b). Therefore, the sensitivity analysis suggests that the near vertical moderately conductive features C_1, and C_2 appear within the highly resistive basement are not artefacts of 2D inversion; rather required by the data.

Discussion and conclusion

In a subsurface resistivity section, a fault zone, in general, exhibits itself as a conductive feature compared to the surrounding region; and the reason for this conductive signature can be attributed to several aspects. Since, our study area is seismically active and the fault zone has a tremendous role on earthquake genesis, therefore, the moderately conductive near vertical features across the basement (C_1, C_2 in Fig. 7) might be considered as basement fault zones. For better precision, we have projected the earthquake hypocenters ($M > 1$), that are falling within a 500 m radius zone centred by the profile, on the 2D resistivity section (Fig. 10a). We have also projected the Donachiwada fault (fault configurations are taken from Gupta et al. 1999), as the profile runs across the fault (Fig. 10a). The correlation of Donachiwada fault with C_1 (Fig. 10a), as well as the alignment of hypocenters along the resistive–conductive boundary (Fig. 10a), clearly indicates that the moderately conductive feature C_1 is Donachiwada fault. Besides, the association of the M 6.3 December 10, 1967 earthquake (Chandra 1976) with the resistive–conductive boundary (Fig. 10a) strongly supports our observation. For the moderately conductive signature C_2, we have a few earthquake hypocenters aligned along the resistive–conductive boundary below a depth of 10 km (Fig. 10a). This observation signifies that the signature C_2 might represent a less active (as compared to the Donachiwada fault) basement fault in Koyna region.

The most favourable explanation for the conductive features obtained in the inversion output of a seismically active zone is the presence of fluid in the fault zone (Mackie et al. 1997; Ogawa and Honkura 1997; Unsworth et al. 1997, 1999), since a little amount of fluid associated with a rock matrix is capable of reducing its bulk resistivity considerably (Gueguen and Palciauskas 1994). However, the consideration of fluid in the fault zone based on the conductivity contrast is still ambiguous because,
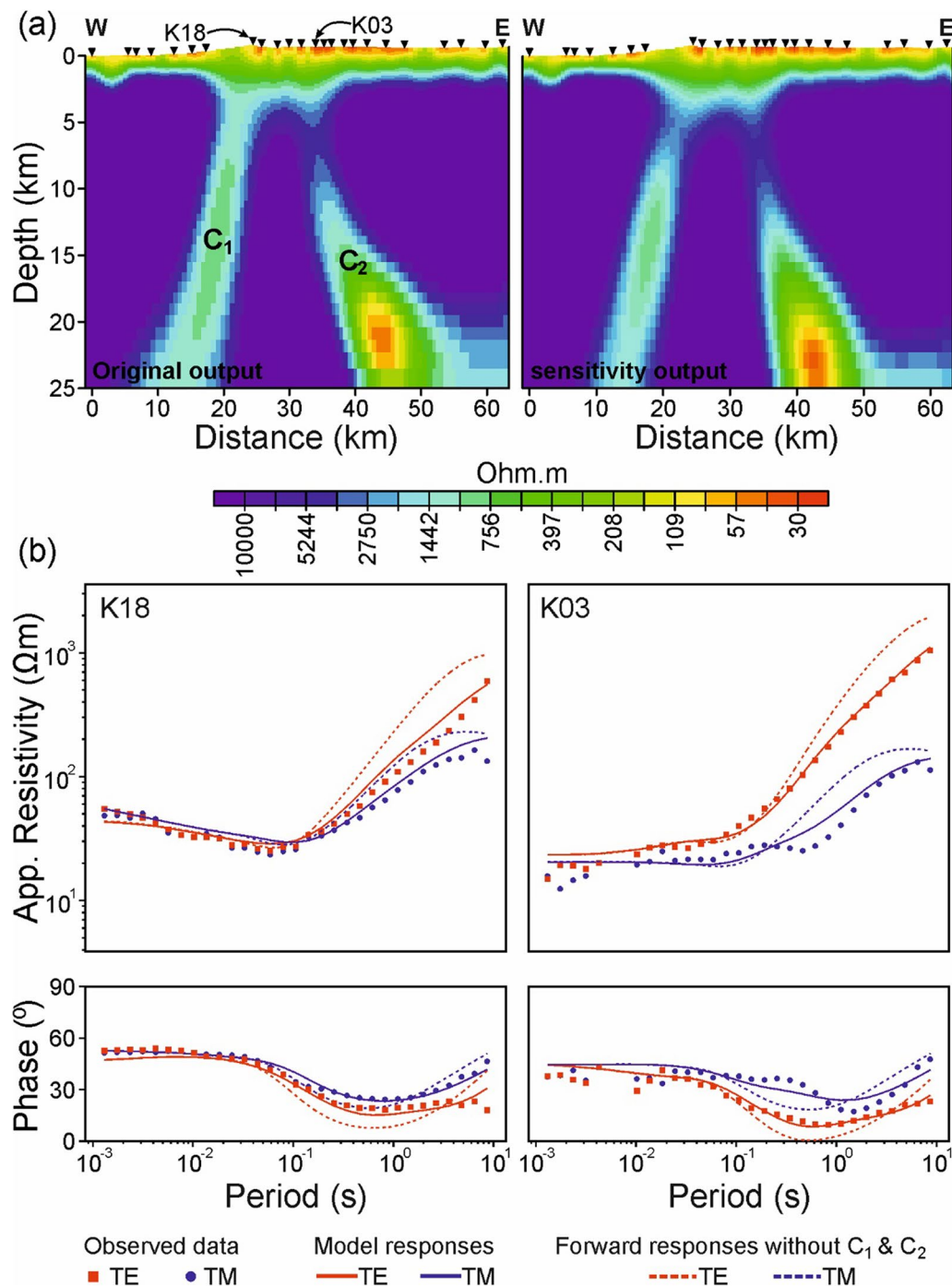
Fig. 9 **a** Comparison of the 2D inversion output along profile-K with the output from sensitivity analysis. Both the outputs represent similar signatures which prove the existence of the near vertical moderately conductive features (C_1, and C_2). **b** Comparison between model responses and the forward responses (obtained without C_1, and C_2, observed in 2D inversion output of profile-K) with data for the sites near to C_1, and C_2 (K18, K03). Data fit degrades when C_1, and C_2 are absent which proves the existence of C_1, and C_2

similar kind of scenario is observed in case of mineralization by chemical precipitation, i.e. ore coated fracture (Becken et al. 2011) and clayey fault gauge (Palacky 1987; Eberhart-Phillips et al. 1995). Therefore, to elucidate the

proper cause for the observed conductivity of C_1 and C_2 we have considered the corresponding ratio of seismic P- to S-wave velocity (v_p/v_s ratio). We convert the resistivity values of each grid point of the resistivity section to its
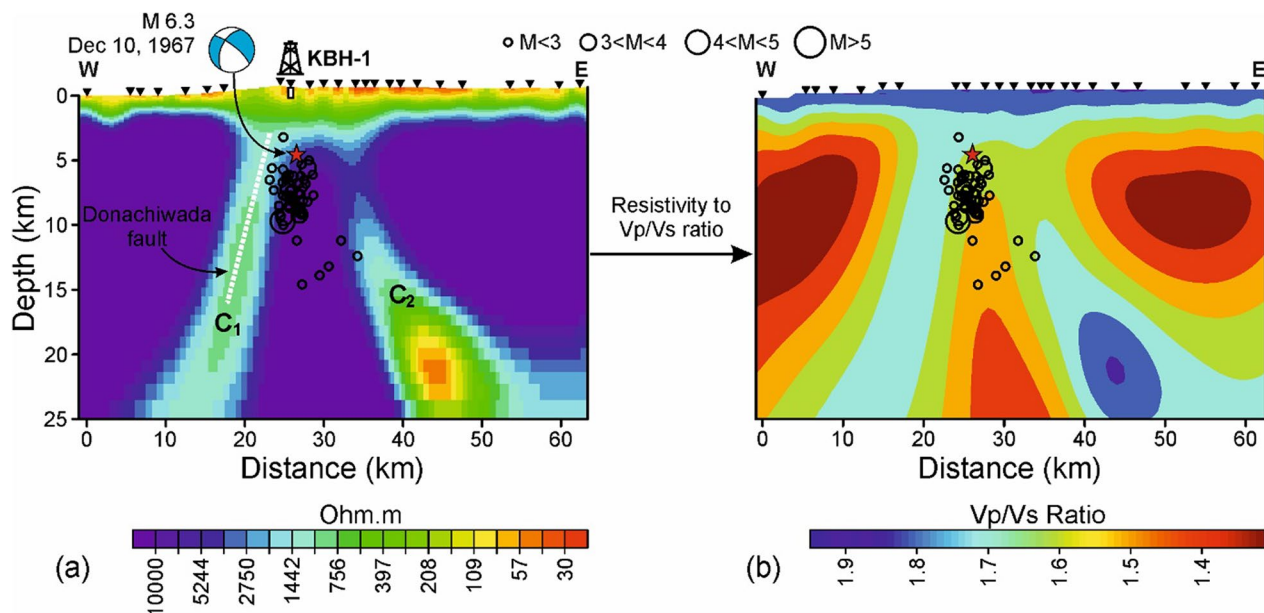
Borah *et al. Earth, Planets and Space*   (2023) 75:149

Page 10 of 14

Fig. 10 **a** Correlation of the projected Donachiwada fault (Gupta et al. 1999) with C_1; the association of the December 10, 1967 (M 6.3) earthquake which occurred near to profile-K and the alignment of projected earthquake hypocenters (black circles), falling within 500 m radius zone centred by the profile with the resistive–conductive boundaries reveal the presence of basement fault. **b** Conversion of resistivity to v_p/v_s ratio using log-linear relationship of Borah and Patro (2022). Association of the earthquake hypocenters with the high v_p/v_s zone than the surroundings signifies the presence of fluid

corresponding v_p/v_s values utilizing the log-linear relationship between resistivity and v_p/v_s (developed for the Koyna region; Borah and Patro 2022) and constructed the corresponding v_p/v_s section (Fig. 10b).

Several studies have established that there is a reduction in seismic wave velocities (both v_p and v_s) within a fault zone because of the reduction in shear modulus of the faulted rocks (Nur and Simmons 1969; Dixit et al. 2014). However, when the faulted rocks are saturated with fluid, v_p increases significantly and v_s remains the same or slightly decreases because of the presence of fluid (Nur and Simmons 1969; O'Connell and Budiansky 1974; Dixit et al. 2014). Such situation results in increase of v_p/v_s in the fluid-saturated fault zone. Therefore, for the shearing of dry rock, one would expect the hypocenters to coincide with regions of low-v_p and low-v_s and the association of hypocenters with high v_p/v_s (high v_p and low v_s) likely signifies the water saturation and high pore pressure within the fault zones (Dixit et al. 2014).

From the v_p/v_s section (Fig. 10b) it is observed that the fault zones C_1, and C_2 (or the earthquake hypocenters) are associated with the regions having high v_p/v_s values (i.e. high v_p and low v_s) w.r.t the surroundings. Therefore, this observation directly points that the conductivity contrast observed in the fault zones (C_1, C_2) is because of the presence of the fluid in the fault zone and rules out the effects of other factors. On the other hand, the evidence

of hydrous alteration along the fault zone (observed from drilling result, Gupta et al. 2017) signifies the water channelization through the fault (Misra et al. 2017) and therefore, supports the presence of fluid in the fault zone.

The resistivity of aqueous fluids depends on temperature and salinity (Becken et al. 2011). In KSZ, the
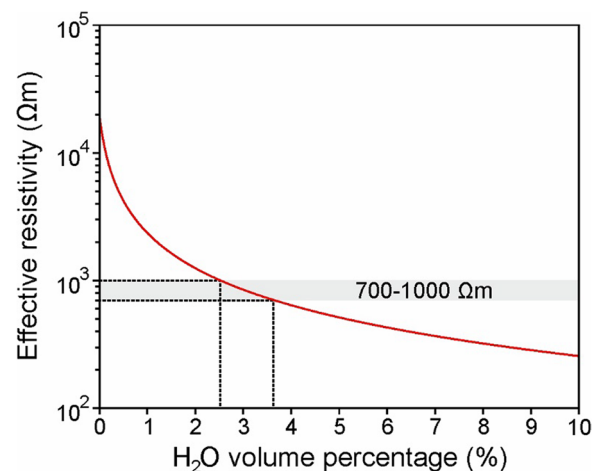

Fig. 11 Plotting of Hashin–Shtrikman upper bound (Hashin and Shtrikman 1962) for two-phase system composed of rock matrix ($\geq 20{,}000$ Ωm) and fluid (~18 Ωm) provides ~2.5–3.6 vol% fluid for ~700–1000 Ωm observed resistivity

Borah *et al. Earth, Planets and Space*   (2023) 75:149
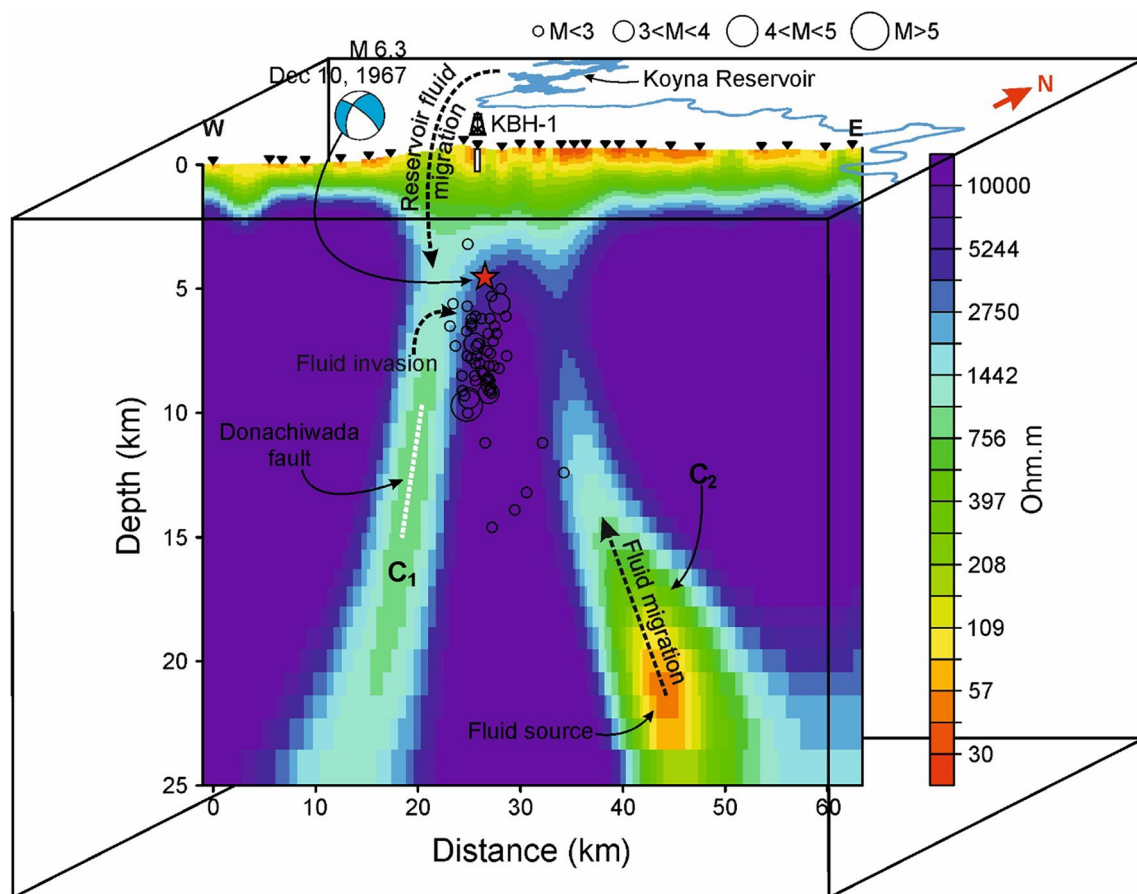
Page 11 of 14

Fig. 12 2D inversion output from joint inversion of TE and TM data along profile-K using NLCG algorithm of Rodi and Mackie (2001) up to 25 km depth brings out an anomalous conductive feature of ~ 40 Ωm below 20 km depth. This conductive feature might signify the presence of dehydrated fluid which has a probable role on the observed seismicity in KSZ along with the meteoric water circulation due to the nearby Koyna reservoir

average estimated temperature for the depth range 6–10 km is 140–195 °C (Gupta et al 2015). The pressure exerted by the granitic basement (of average density ~ 2.65 g cm^{-3} Gupta et al. 2017) at this depth range is 1558–2597 bars. Therefore, for this temperature and pressure range the estimated average density of pure water (Burnham et al. 1969) at 6–10 km depth range is ~ 0.988 g cm^{-3}. The hydrochemical study on the well water of Koyna region (Reddy et al. 2017) suggests a very low salt (Cl$^-$) content of maximum 30 mg L^{-1} (or 0.003 wt%). Therefore, for the temperature range 140–195 °C, the average resistivity of aqueous fluid (ρ_f) of density 0.988 g cm^{-3} containing 0.003 wt% salt (Cl$^-$) will be ~ 18 Ωm (Sinmyo and Keppler 2017). For this two-phase system of very highly resistive rock matrix ($\geq$ 20,000 Ωm) and a low resistive fluid phase (~ 18 Ωm), the Hashin–Shtrikman upper bound (Hashin and Shtrikman 1962) suggests ~ 2.5–3.6 vol%

of interconnected fluid (Fig. 11) to explain the observed bulk resistivity (ρ_b) of ~ 700–1000 Ωm for C_1, and C_2.

The minimum interconnected porosity (Φ) filled with fluid of resistivity ρ_f (~ 18 Ωm) that is required to explain the observed bulk resistivity (ρ_b) of ~ 700–1000 Ωm solely due to the fluid phase (i.e. $S_w = 1$, S_w is the pore space filled by water with a resistivity ρ_f) can be estimated using Archie's law, $\rho_b = \rho_f \Phi^{-m}$; where m is the cementation exponent of the rock and usually ranges between 1 to 2. The lower bound of m ($m = 1$) is more capable of furnishing reasonable and desirable porosity estimations for fault zones (Unsworth et al. 1997). Therefore, considering that only the fluid conductivity (18 Ωm) contributes to the bulk rock conductivity (700–1000 Ωm), we estimate the corresponding interconnected porosity and found that ~ 1.8–2.6% interconnected porosity is responsible for the observed bulk resistivity of ~ 700–1000 Ωm of C_1 and C_2.

Borah *et al. Earth, Planets and Space* (2023) 75:149

Page 12 of 14

Several previous studies have pointed out the correlation of the observed seismicity with the loading and unloading of nearby Koyna reservoir. Therefore, the meteoric water circulation through existing faults in the basement, due to the loading of the reservoir, may consider as the potential fluid source for the fault zone (Fig. 12). However, the present MT investigation has sensed a conductive feature of ~ 40 Ωm below a depth of 20 km (Fig. 12). The existence of this anomalous conductive feature is affirmed by the sensitivity analysis (Fig. 9a). This conductive zone has a linkage to the upper crust through C_2 (Fig. 12). This conductive zone hints towards the probable presence of a fluid source; since aqueous fluids can be found at mid to lower crustal depths due to the dehydration of amphibole bearing rocks at ≥ 600 °C (Vanyan and Gliko 1999). Amphibole, one of the important hydrous mineral in the continental middle crust (Wang et al. 2012) is abundant (35–40%) in the depth range of 15–30 km (Christensen and Mooney 1995). The temperature–depth profile of KSZ (Gupta et al. 2015) suggests a temperature of ~ 600 °C at 25–30 km depth (considering ~ 50 mWm^{-2} surface heat flux and ~ 0.5 μWm^{-3} heat production for the granite-gneiss) which is favourable for the dehydration. Therefore, there is a possibility for dehydrated fluid source below 20 km depth and upward fluid movement from this source due to buoyancy (Becken and Ritter 2012), through the conductive pathway (C_2), to provide a linkage between the fluid source and upper crust (Fig. 12). In this perspective, C_2 might be considered as fluid migration path (from lower crustal depth to upper crustal depth) rather than a basement fault.

It is interesting to observe that the hypocenters are aligned along the resistive–conductive block boundaries and associated with the resistive basement blocks (Figs. 10 and 12). It is observed that the fault zone fluid at hydrostatic pressure suppresses seismicity and over-pressurised fluid tends to induce seismicity (Becken and Ritter 2012). This observation signifies that the hydraulically interconnected fault zone fluid at hydrostatic pressure makes the fault zone conductor too weak to accumulate the necessary shear stress for brittle failure (Ritter et al. 2005; Unsworth et al. 2000). Generally, in case of fluid-induced seismicity, the high pressurized fluid (sourced in the conductive zones due to the loading of reservoir and deeper fluid source) invades the critically stressed surrounding resistive formations, lowers the shear stress required for failure, and thereby facilitates the mechanical failure within the rheologically strong regions nearby (Jiracek et al. 2007; Sleep and Blanpied 1992).

The observed alignment of the earthquake hypocenters within the resistive basement block of the resistive–conductive block boundaries (Fig. 12) can therefore be explained by the invasion of fluid (Gurer and Bayrak 2007) from conductive mechanically weak permeable zones (C_1, C_2) to resistive (less permeable) mechanically strong zone along the structural boundary (Fig. 12). This migration induces high fluid pressure that leads to brittle rock failure (Becken et al. 2011) within the high resistivity basement block near the resistive–conductive boundaries (Fig. 12). The entire process depends on the stress concentration and the fluid penetration depth into the resistive rocks (Becken et al. 2011).

Supplementary Information

The online version contains supplementary material available at https://doi.org/10.1186/s40623-023-01905-5.

Additional file 1. Fig. S1: Data in terms of apparent resistivity and phase used in the present study.

Declarations

Competing interests

The authors declare that they have no known competing financial interests or personal relationships that could have appeared to influence the work reported in this paper.

Author details

[1]Gauhati University, Gopinath Bordoloi Nagar, Jalukbari, Guwahati 781014, India. [2]CSIR-National Geophysical Research Institute, Uppal Road, Hyderabad 500007, India. [3]Andhra University, Waltair Junction, Visakhapatnam 530003, India. [4]Università degli studi di Bari Aldo Moro, 70121 Bari BA, Italy.

References

Athavale RN, Mohan I (1976) A technical report on integrated geophysical studies in the Koyna hydroelectric project area of maharashtra state. Technical report, CSIR-NGRI and CEG

Bahr K (1988) Interpretation of the magnetotelluric impedance tensor: regional induction and local telluric distortion. J Geophys 62:119–127

Bahr K (1991) Geological noise in magnetotelluric data: a classification of distortion types. Phys Earth Planet Inter 66:24–38. https://doi.org/10.1016/0031-9201(91)90101-M

Beamish D, Travassos JM (1992) The use of the D$^+$ solution in magnetotelluric interpretation. J Appl Geophys 29:1–19. https://doi.org/10.1016/0926-9851(92)90009-A

Becken M, Burkhardt H (2004) An ellipticity criterion in magnetotelluric tensor analysis. Geophys J Int 159:69–82. https://doi.org/10.1111/j.1365-246X.2004.02376.x

Becken M, Ritter O (2012) Magnetotelluric studies at the san andreas fault zone: implications for the role of fluids. Surv Geophys 33:65–105. https://doi.org/10.1007/s10712-011-9144-0

Becken M, Ritter O, Bedrosian PA, Weckmann U (2011) Correlation between deep fluids, tremor and creep along the central San Andreas fault. Nature 480:87–90. https://doi.org/10.1038/nature10609

Borah UK, Patro PK (2019) Estimation of the depth of investigation in the magnetotelluric method from the phase. Geophysics 84:E377–E385. https://doi.org/10.1190/geo2018-0124.1

Borah UK, Patro PK (2022) The interrelationship between electrical resistivity and v_p/v_s ratio: a novel approach to constrain the subsurface resistivity structure in data gap areas in a seismogenic zone. Geophysics 87:B57–B67. https://doi.org/10.1190/geo2021-0200.1

Borah UK, Patro PK, Suresh V (2015) Processing of noisy magnetotelluric time series from Koyna-Warna seismic region, India: a systematic approach. Ann Geophys 58:G0222. https://doi.org/10.4401/ag-6690

Burgmann R, Dresen G (2008) Rheology of the lower crust and upper mantle: evidence from rock mechanics, geodesy, and field observations. Ann Rev Earth Planet Sci 36:531–567. https://doi.org/10.1146/annurev.earth.36.031207.124326

Burnham CW, Holloway JR, Davis NF (1969) Thermodynamic properties of water to 1000 °C and 10000 bars. Geol Soc Am Spec Pap 132:1–96. https://doi.org/10.1130/SPE132

Caldwell TG, Bibby HM, Brown C (2004) The magnetotelluric phase tensor. Geophys J Int 158:457–469. https://doi.org/10.1111/j.1365-246X.2004.02281.x

Chandra U (1976) Focal mechanism of the Koyna, India earthquake of 1967, December 10. Geophys J Int 46:247–251. https://doi.org/10.1111/j.1365-246X.1976.tb04156.x

Chen X, Nakata N, Pennington C, Haffener J, Chang JC, He X, Zhan Z, Ni S, Walter JI (2017) The Pawnee earthquake as a result of the interplay among injection, faults and foreshocks. Sci Rep 7:4945. https://doi.org/10.1038/s41598-017-04992-z

Christensen NI, Mooney WD (1995) Seismic velocity structure and composition of the continental crust: a global view. J Geophys Res 100:9761–9788. https://doi.org/10.1029/95JB00259

Constable SC, Parker RL, Constable CG (1987) Occam's inversion: a practical algorithm for generating smooth models from electromagnetic sounding data. Geophysics 52:289–300. https://doi.org/10.1190/1.1442303

Dixit MM, Kumar S, Catchings RD, Suman K, Sarkar D, Sen MK (2014) Seismicity, faulting, and structure of the Koyna-Warna seismic region, Western India from local earthquake tomography and hypocenter locations. J Geophys Res 119:6372–6398. https://doi.org/10.1002/2014JB010950

Duncan RA, Pyle DG (1988) Rapid eruption of Deccan flood basalts at the Cretaceous/Tertiary boundary. Nature 333:841–843. https://doi.org/10.1038/333841a0

Eberhart-Phillips D, Stanley WD, Rodriguez BD, Lutter WJ (1995) Surface seismic and electrical methods to detect fluids related to faulting. J Geophys Res 100:12919–12936. https://doi.org/10.1029/94JB03256

Fulton PM, Saffer DM (2009) Potential role of mantle-derived fluids in weakening the San Andreas Fault. J Geophys Res 114:B07408. https://doi.org/10.1029/2008JB006087

Goswami D, Hazarika P, Roy S (2020) In situ stress orientation from 3 km borehole image logs in the Koyna Seismogenic Zone, Western India: implications for transitional faulting environment. Tectonics 39:e2019TC005647. https://doi.org/10.1029/2019TC005647

Gowd TN, Rao SVS, Gaur VK (1992) Tectonic stress field in the Indian subcontinent. J Geophys Res 97:11879–11888. https://doi.org/10.1029/91JB03177

Groom RW, Bailey RC (1989) Decomposition of magnetotelluric impedance tensors in the presence of local three dimensional galvanic distortion. J Geophys Res 94:1913–1925. https://doi.org/10.1029/JB094iB02p01913

Gueguen Y, Palciauskas V (1994) Introduction to the physics of rocks. Princeton University Press, New York

Guha SK, Gosavi PD, Varma MM, Agarwal SP, Padale JG, Marwadi SC (1968) Recent seismic disturbances in the Koyna Hydroelectric Project, Maharashtra, India. Technical report, Central Water and Power Research Station, Pune

Gupta HK (1983) Induced seismicity hazard mitigation through water level manipulation at Koyna, India: a suggestion. Bull Seismol Soc Am 73:679–682

Gupta H (2002) A review of recent studies of triggered earthquakes by artificial water reservoirs with special emphasis on earthquakes in Koyna, India. Earth Sci Rev 58:279–310. https://doi.org/10.1016/S0012-8252(02)00063-6

Gupta H (2011) Artificial water reservoir triggered earthquakes. In: Gupta H (ed) Encyclopedia of solid earth geophysics. Springer, Berlin. https://doi.org/10.1007/978-90-481-8702-7_15

Gupta HK, Rastogi BK (1974) Will another damaging earthquake occur in Koyna? Nature 248:215–216. https://doi.org/10.1038/248215a0

Gupta HK, Rastogi BK (1976) Dams and earthquake. Elsevier, Amsterdam

Gupta HK, Narain H, Rastogi BK, Mohan I (1969) A study of the Koyna earthquake of December 10, 1967. Bull Seismol Soc Am 59:1149–1162

Gupta HK, Rastogi BK, Narain H (1972a) Common features of the reservoir associated seismic activities. Bull Seismol Soc Am 62:481–492

Gupta HK, Rastogi BK, Narain H (1972b) Some discriminatory characteristics of earthquakes near the Kariba, Kremasta and Koyna artificial lakes. Bull Seismol Soc Am 62:493–507

Gupta HK, Rao RUM, Srinivasan R, Rao GV, Reddy GK, Dwivedy KK, Banerjee DC, Mohanty R, Satyasaradhi YR (1999) Anatomy of surface rupture zones of two stable continental region earthquakes, 1967 Koyna and 1993 Latur, India. Geophys Res Lett 26:1985–1988. https://doi.org/10.1029/1999GL900399

Gupta HK, Mandal P, Rastogi BK (2002) How long will triggered earthquakes at Koyna, India continue? Curr Sci 82:202–210

Gupta HK, Rao NP, Roy S, Arora K, Tiwari VM, Patro PK, Satyanarayana HVS, Shashidhar D, Mallika K, Akkiraju VV, Goswami D, Vyas D, Ravi G, Srinivas KNSSS, Srihari M, Mishra S, Dubey CP, Raju DCV, Borah U, Reddy KC, Babu N, Rohilla S, Dhar U, Sen M, Rao YJB, Bansal BK, Nayak S (2015) Investigations related to scientific deep drilling to study reservoir-triggered earthquakes at Koyna, India. Int J Earth Sci 104:1511–1522. https://doi.org/10.1007/s00531-014-1128-0

Gupta HK, Arora K, Rao NP, Roy S, Tiwari V, Patro PK, Satyanarayana HVS, Shashidhar D, Mahato CR, Srinivas KNSSS, Srihari M, Satyavani N, Srinu Y, Gopinadh D, Raza H, Jana M, Akkiraju VV, Goswami D, Vyas D, Dubey CP, Raju DCV, Borah U, Raju K, Reddy KC, Babu N, Bansal BK, Nayak S (2017) Investigations of continued reservoir triggered seismicity at Koyna, India. In: Mukherjee S, Misra AA, Calves G, Nemcok M (eds) Tectonics of the Deccan large igneous province. Geological Society of London, London

Gurer A, Bayrak M (2007) Relation between electrical resistivity and earthquake generation in the crust of West Anatolia, Turkey. Tectonophysics 445:49–65. https://doi.org/10.1016/j.tecto.2007.06.009

Hansen PC (1998) Rank deficient and discrete Ill: posed problems, numerical aspects of linear inversion. Society for Industrial and Applied Mathematics, Philadelphia. https://doi.org/10.1137/1.9780898719697

Hashin Z, Shtrikman S (1962) A variational approach to the theory of effective magnetic permeability of multiphase materials. J Appl Phys 33:3125–3131. https://doi.org/10.1063/1.1728579

Irwin WP, Barnes I (1980) Tectonic relations of carbon-dioxide discharges and earthquakes. J Geophys Res 85:3115–3121. https://doi.org/10.1029/JB085iB06p03115

Jiracek GR, Gonzalez VM, Caldwell TG, Wannamaker PE, Kilb D (2007) Seismogenic, electrically conductive, and fluid zones at continental plate boundaries in New Zealand, Himalaya, and California, USA. In: Okaya D, Stern T, Davey F (eds) A continental plate boundary: tectonics at South Island, New Zealand. Geophysical Monogaph Series, AGU. https://doi.org/10.1029/175GM18

Borah *et al. Earth, Planets and Space*   (2023) 75:149

Page 14 of 14

Jones AG (2012) Distortion of magnetotelluric data: its identification and removal. In: Chave AD, Jones AG (eds) The magnetotelluric method, theory and practice. Cambridge University Press, Cambridge. https://doi.org/10.1017/CBO9781139020138.008

Jones AG, Hutton R (1979) A multi-station magnetotellurics study in southern Scotland-II. Monte-Carlo inversion of the data and its geophysical and tectonic implications. Geophys J Int 56:351–368. https://doi.org/10.1111/j.1365-246X.1979.tb00169.x

Kailasam LN, Reddy AGB, Sathyamurthy KRJ, Murthy BSR (1976) Deep electrical resistivity soundings in Deccan trap region. Curr Sci 45:9–13

Krishna Brahmam N, Negi JG (1973) Rift valleys beneath the Deccan trap (India). Geophys Res Bull 11:207–237

Langston CA, Franco-Spera M (1985) Modeling of Koyna India, aftershock of 12th December 1967. Bull Seismol Soc Am 75:651–660

Mackie RL, Livelybrooks DW, Madden TR, Larsen JC (1997) A magnetotelluric investigation of the San Andreas fault at Carrizo plain, California. Geophys Res Lett 24:1847–1850. https://doi.org/10.1029/97GL01604

McNeice GW, Jones AG (2001) Multisite, multifrequency tensor decomposition of magnetotelluric data. Geophysics 66:158–173. https://doi.org/10.1190/1.1444891

Miller SA (2013) The role of fluids in tectonic and earthquake processes. In: Dmowska R (ed) Advances in geophysics. Elsevier, Amsterdam. https://doi.org/10.1016/B978-0-12-380940-7.00001-9

Misra S, Bartakke V, Athavale G, Akkiraju VV, Goswami D, Roy S (2017) Granite-gneiss basement below Deccan Traps in the Koyna region, western India: Outcome from Scientific Drilling. J Geol Soc India 90:776–782. https://doi.org/10.1007/s12594-017-0790-9

Narain H, Gupta H (1968a) Observations on Koyna earthquake. J Indian Geophys Union 5:30–34

Narain H, Gupta H (1968b) The Koyna earthquake. Nature 217:1138–1139. https://doi.org/10.1038/2171138a0

Nur A, Simmons G (1969) The effect of saturation on velocity in low porosity rocks. Earth Planet Sci Lett 7:183–193. https://doi.org/10.1016/0012-821X(69)90035-1

O'Connell RJ, Budiansky B (1974) Seismic velocities in dry and saturated cracked solids. J Geophys Res 79:5412–5426. https://doi.org/10.1029/JB079i035p05412

Ogawa Y, Honkura Y (1997) An audiomagnetotelluric view of the Atera fault. J Geomagn Geoelectr 49:1065–1071. https://doi.org/10.5636/jgg.49.1065

Oldenburg DW, Whittal KP, Parker RL (1984) Inversion of ocean bottom magnetotellurics data revisited. J Geophys Res 89:1829–1833. https://doi.org/10.1029/JB089iB03p01829

Palacky GJ (1987) Resistivity characteristics of geologic targets. In: Nabighian MN (ed) Electromagnetic methods in applied geophysics—theory. Exploration geophysics, Tulsa, Okla, vol 1, pp 53–129. https://doi.org/10.1190/1.9781560802631.ch3

Pandey AP, Chadha RK (2003) Surface loading and triggered earthquakes in the Koyna-Warna region, western India. Phys Earth Planet Interior 139:207–223. https://doi.org/10.1016/j.pepi.2003.08.003

Parker RL, Whaler KA (1981) Numerical methods for establishing solutions to the inverse problem of electromagnetic induction. J Geophys Res 86:9574–9584. https://doi.org/10.1029/JB086iB10p09574

Patro PK, Sarma SVS (2009) Lithospheric electrical imaging of the Deccan trap covered region of western India. J Geophys Res 114:B01102. https://doi.org/10.1029/2007JB005572

Reddy DV, Kumar D, Rao NP (2017) Long-term hydrochemical earthquake precursor studies at the Koyna-Warna Reservoir Site in Western India. J Geol Soc India 90:720–727. https://doi.org/10.1007/s12594-017-0781-x

Ritter O, Hoffmann-Rothe A, Bedrosian PA, Weckmann U, Haak V (2005) Electrical conductivity images of active and fossil fault zones. In: Bruhn D, Burlini L (eds) In high-strain zones: structure and physical properties, Geological Society of London Special Publications, London. https://doi.org/10.1144/GSL.SP.2005.245.01.08

Rodi W, Mackie RL (2001) Nonlinear conjugate gradients algorithm for 2-D magnetotelluric inversions. Geophysics 66:174–187. https://doi.org/10.1190/1.1444893

Roy S, Rao NP, Akkiraju VV, Goswami D, Sen M (2013) Granitic basement below Deccan Traps unearthed by drilling in the Koyna seismic zone, western India. J Geol Soc India 81:289–290. https://doi.org/10.1007/s12594-013-0034-6

Sarma SVS, Patro BPK, Harinarayana T, Veeraswamy K, Sastry RS, Sarma MVC (2004) A magnetotelluric (MT) study across the Koyna seismic zone, western India: evidence for block structure. Phys Earth Planet Interior 142:23–36. https://doi.org/10.1016/j.pepi.2003.12.005

Schilling FR, Partzsch GM (2001) Quantifying partial melt fraction in the crust beneath the central Andes and the Tibetan plateau. Phys Chem Earth Part A 26:239–246. https://doi.org/10.1016/S1464-1895(01)00051-5

Shashidhar D, Rao NP, Srinagesh D, Gupta H, Satyanarayana HVS, Suresh G, Satish A (2013) The 14 April 2012 Koyna Earthquake of Mw 4.8: insights into active tectonics of the Koyna region. J Seismolog 17:1345–1353. https://doi.org/10.1007/s10950-013-9396-x

Simpson F, Bahr K (2005) Practical magnetotellurics. Cambridge University Press, Cambridge. https://doi.org/10.1017/CBO9780511614095

Sinmyo R, Keppler H (2017) Electrical conductivity of NaCl bearing aqueous fluids to 600 °C and 1 GPa. Contrib Miner Petrol 172:4. https://doi.org/10.1007/s00410-016-1323-z

Sleep NH, Blanpied ML (1992) Creep, compaction and the weak rheology of major faults. Nature 359:687–692. https://doi.org/10.1038/359687a0

Smith JT (1995) Understanding telluric distortion matrices. Geophys J Int 122:219–226. https://doi.org/10.1111/j.1365-246X.1995.tb03549.x

Smith JT (1997) Estimating galvanic-distortion magnetic fields in magnetotellurics. Geophys J Int 130:65–72. https://doi.org/10.1111/j.1365-246X.1997.tb00988.x

Swift CM Jr (1967) A magnetotelluric investigations of electrical conductivity anomaly in the southwestern United States. Dissertation, Massachusetts Institute of Technology

Talwani P (1997) Seismotectonics of the Koyna-Warna area, India. Pure Appl Geophys 150:511–550. https://doi.org/10.1007/s000240050091

Tikhonov AN, Arsenin VY (1977) Solutions of Ill-posed problems. Winston and Sons, Washington, DC

Unsworth MJ, Malin PE, Egbert GD, Booker JR (1997) Internal structure of the San Andreas fault zone at Parkfield, California. Geology 25:359–362. https://doi.org/10.1130/0091-7613(1997)025%3c0359:ISOTSA%3e2.3.CO;2

Unsworth MJ, Egbert GD, Booker JR (1999) High-resolution electromagnetic imaging of the San Andreas fault in Central California. J Geophys Res 104:1131–1150. https://doi.org/10.1029/98JB01755

Unsworth MJ, Bedrosian P, Eisel M, Egbert G, Siripunvaraporn W (2000) Along strike variations in the electrical structure of the San Andreas Fault at Parkfield, California. Geophys Res Lett 27:3021–3024. https://doi.org/10.1029/2000GL011476

Vanyan LL, Gliko AO (1999) Seismic and electromagnetic evidence of dehydration as a free water source in the reactivated crust. Geophys J Int 137:159–162. https://doi.org/10.1046/j.1365-246x.1999.00767.x

Wang D, Guo Y, Yu Y (2012) Electrical conductivity of amphibole-bearing rocks: influence of dehydration. Contribut Mineral Petrol 164:17–25. https://doi.org/10.1007/s00410-012-0722-z

Publisher's Note

Springer Nature remains neutral with regard to jurisdictional claims in published maps and institutional affiliations.